SPUMIC: SIMULTANEOUS PHASE UNWRAPPING AND MULTIPATH INTERFERENCE CANCELLATION IN TIME-OF-FLIGHT CAMERAS USING SPECTRAL METHODS

Ahmed Kirmani *

Massachusetts Institute of Technology
Cambridge, MA 02139

Arrigo Benedetti

Microsoft Corporation
Mountain View, CA 94043

Philip A. Chou †

Microsoft Research
Redmond, WA 90048

ABSTRACT

We propose a framework for simultaneous phase unwrapping and multipath interference cancellation (SPUMIC) in homodyne time-of-flight (ToF) cameras. Our multi-frequency acquisition framework is based on parametric modeling of the multipath interference phenomena. We use robust spectral estimation methods with low computational complexity to detect and estimate multipath parameters. Using simulations and analysis we demonstrate that our proposed solution is implementable in real-time on existing ToF cameras without requiring any hardware modifications.

Index Terms— Time-of-flight range imaging, depth sensing, 3D camera, phase unwrapping, multipath cancellation, mixed, flying pixel, spectral estimation.

1. INTRODUCTION

Time-of-flight (ToF) depth cameras enable real-time acquisition of three-dimensional (3D) scene structure with high range resolution from a single viewpoint. They are also less sensitive to ambient light compared to their active stereo and structured light counterparts. Due to these desirable features, ToF cameras are being rapidly integrated into an array of applications including navigation, automation and consumer electronics [1]. Development of new image and signal processing techniques to improve ToF range imaging quality is also subject to growing research interest.

Range imaging using homodyne ToF cameras [2] presents two fundamental challenges: phase unwrapping and multipath interference cancellation. With the growing deployment of ToF cameras, these two problems have recently received significant attention [3, 4, 5, 6, 7, 8, 9, 10]. Thus far, phase unwrapping (PUW) and multipath interference cancellation (MIC) have been investigated independently and several methods have been proposed for each one. Moreover, for both these problems there is a lack of solutions that work in real time as well as produce accurate range estimates in the presence of signal dependent shot noise experienced by ToF measurements.

In this paper, we jointly address PUW and MIC in ToF cameras using the theory of spectral estimation. Our integrated solution, SPUMIC, is a pointwise multipath detection and parameter estimation framework. SPUMIC is based on multi-frequency ToF acquisition and parametric modeling of multipath signals. Our measurement process involves sampling cross-correlation functions at five or more uniformly spaced modulation frequencies. For every sensor pixel, SPUMIC first detects the presence or absence of multipath and then estimates the unwrapped distance and amplitude parameters.

Our analysis and simulations demonstrate that SPUMIC

1. produces accurate depth estimates of the direct scene path in presence of signal dependent noise, and
2. is implementable in real-time on existing ToF cameras without requiring hardware modifications.

We proceed as follows: in Section 2 we explain the theory of ToF camera operation, in Section 3 we discuss parametric modeling of multipath interference in ToF cameras and in Section 4, we present our joint framework for PUW and MIC. We conclude with analysis and simulations of our method in Section 5.

2. TIME-OF-FLIGHT CAMERA OPERATION

Figure 1 shows a signal processing abstraction of the operation of a amplitude modulated cosine wave (AMCW) homodyne ToF camera. The radiant power of transmitted light is temporally modulated using a non-negative sinusoidal signal

$$s(t) = s(t+T_0) = 1+\cos 2\pi f_0 t \qquad (1)$$

with modulation frequency $f_0 = 1/T_0$. In the absence of multipath interference, the reflected light from the scene is well modeled as

$$r(t) = r(t+T_0) = a\ \cos 2\pi f_0(t-\tau)+(a+b), \qquad (2)$$

where a is the amplitude attenuation due to propagation losses and target reflectivity; $\tau = 2d/c$ is the time-delay introduced due to the to and fro propagation of light with speed c from the camera to a scene point at distance d, and b is the time-invariant background or ambient light contribution from the

*Department of Electrical Engineering and Computer Science at MIT. Email: *akirmani at mit.edu*

†Multimedia Interaction and Communication Research group. Email: *pachou at microsoft.com*

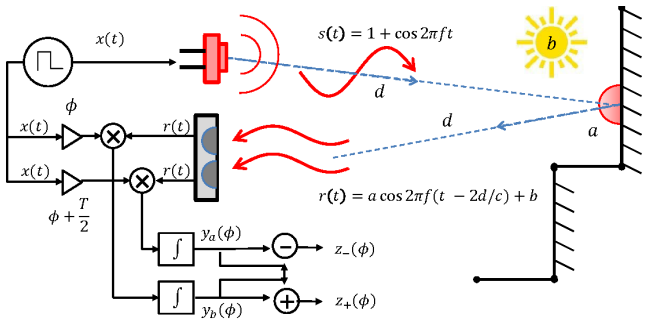

Fig. 1. Signal processing pipeline of ToF camera operation.

scene. Our goal is to estimate a and the unwrapped distance d.

In a homodyne ToF camera, the light signal, $r(t)$, incident at the sensor pixel is correlated with a periodic reference signal, $x(t+\phi) = x(t+\phi+T_0)$, and its time-shifted copy, $x(t+\phi+T_0/2)$. The role of the shift parameter, ϕ, will become imminently clear. The reference signal, $x(t)$, is chosen such that

$$\begin{aligned} x(t)+x(t+T_0/2) &\approx 1 \qquad \text{[light flux preservation]} \\ x(t)-x(t+T_0/2) &\approx (-1)^{\text{sign}\{T_0/2-t\}} \text{[background rejection]} \end{aligned} \tag{3}$$

For simplicity we also assume that the second Fourier series coefficient of $x(t)$ corresponding to frequency f_0 is 1. Under the aforementioned conditions, the cross-correlation functions, denoted using y_a and y_b are computed as

$$\begin{aligned} y_a(\phi+\tau) &= \int_0^{T_0} r(t)\, x(t+\phi)\, \mathrm{d}t \\ &= a\, \cos 2\pi f_0(\phi+\tau)+(a+b) \\ y_b(\phi+\tau) &= \int_0^{T_0} r(t)\, x(t+\phi+T_0/2)\, \mathrm{d}t \\ &= -a\, \cos 2\pi f_0(\phi+\tau)+(a+b) \end{aligned} \tag{4}$$

For a fixed value of ϕ, the following values are measured at the output of a ToF sensor pixel,

$$\begin{aligned} z_+(\phi;\tau) &= [y_a+y_b]/2 = a+b \\ z_-(\phi;\tau) &= [y_a-y_b]/2 = a\, \cos 2\pi f_0(\phi+\tau) \end{aligned} \tag{5}$$

Note $z_+(\phi;\tau) = z_+$ is a constant and provides an estimate of the total incident radiant power. The function $z_-(\phi;\tau)$ is a sinusoid with no background component.

To estimate a and τ, we sample $z_-(\phi;\tau)$ at $M \geq 2$ values of ϕ. The m-th sample is $z_-[m;\tau] = a\, \cos 2\pi f_0\,(mT_0/M+\tau)$ for $m = 0,\ldots,M-1$. For modulation frequency, f_0, the amplitude estimate is

$$\hat{a}\,(f_0) = \sqrt{z_-[0;\tau]^2+\ldots+z_-[M-1;\tau]^2}\,/M \tag{6}$$

and an estimate of the wrapped or aliased distance is,

$$\hat{d}\,(f_0) = \frac{1}{2\pi}\left(\frac{cT_0}{2}\right) \arg\left\{\sum_{m=0}^{M-1} z_-[m;\tau]e^{-j\frac{2\pi m}{M}}\right\} = \frac{c\,\varphi(f_0)}{4\pi f_0} \tag{7}$$

2.1. Phase Unwrapping in ToF cameras

The maximum non-wrapped or unaliased distance when using modulation frequency f_0 is $c/(2f_0)$. Thus, one must choose a low modulation frequency to avoid wrapping. However, the error in the distance estimate $\Delta\hat{d}\,(f_0) \propto \Delta\varphi(f_0)/f_0$. Using the noise model in Section 2.2, it is easy to conclude that $\Delta\varphi(f_0) = \Delta\varphi$ is independent of modulation frequency. This immediately implies that the use of a high modulation frequency leads to more accurate distance estimates, although they will be undesirably wrapped. The use of two or more high modulation frequencies allows us to capture high accuracy distance estimates as well as accomplish reliable phase or distance unwrapping [7]. For example, using modulation frequencies, f_0 and f_1, the unwrapped distance estimation problem is the solution of following system of equations in variables $\hat{d} \geq 0$ and $k_1, k_2 \in \{0,1,2,\ldots\}$,

$$\hat{d} = c\,(\varphi(f_0)+2\pi k_0)/4\pi f_0 = c\,(\varphi(f_1)+2\pi k_1)/4\pi f_1 \tag{8}$$

Using two frequencies, the maximum unaliased distance is increased to $c/(2\,\text{gcd}(f_0,f_1))$.

2.2. Modeling Poisson (shot) noise in ToF cameras

It is well known that ToF cameras suffer from signal dependent shot noise [11]. This is because the process of measuring instantaneous light power using semiconductor substrates involves conversion of photon energy to electron displacement. This stochastic process is accurately modeled as a time-inhomogeneous Poisson process [12] with rate $\lambda(t) = \eta\, r(t)$, where η is quantum efficiency of the detector. In order to reduce the effect of shot noise, the cross-correlation samples are averaged over a large number of time-periods, N. Using the central limit theorem, it is easy to conclude that the averaged output at the sensor pixel is distributed as,

$$\begin{aligned} Z_-(\phi;\tau) &\sim \mathcal{N}\left(\eta\, a\, \cos 2\pi f_0(\phi+\tau)\,,\, \eta\,(a+b)/2N\right) \\ Z_+ &\sim \mathcal{N}\left(\eta\,(a+b)\,,\, \eta\,(a+b)/2N\right) \end{aligned} \tag{9}$$

In Section 5 we will use this physically accurate noise model in our simulations to validate the performance of SPUMIC. In the next section, we briefly discuss a parametric model for multipath interference in ToF cameras.

3. MULTIPATH INTERFERENCE MODELING

As shown in Figure 2, multipath interference in ToF camera arises when a sensor pixel receives contributions from two or more scene points at different depths.

There are various signal models for multipath returns [3] but the one that works particularly well in practice models the reflected return as a sum of a first (direct) return and a second (indirect) path, i.e.,

$$\begin{aligned} r(t;\tilde{\tau}) &= a_1 \cos 2\pi f_0(t-\tau_1)+a_2 \cos 2\pi f_0(t-\tau_2)+\tilde{b} \\ &= \tilde{a}\, \cos 2\pi f_0(t-\tilde{\tau})+\tilde{b} \end{aligned} \tag{10}$$

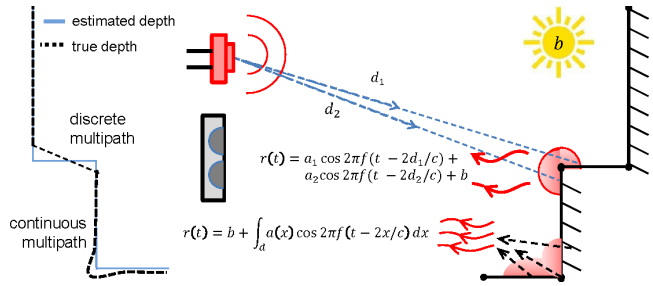

Fig. 2. Mechanism of multipath interference in TOF cameras.

The four multipath parameters of interest are $\{a_1, a_2, d_1, d_2\}$. $\tilde{b} \doteq a_1+a_2+b$ and $\tau_1 = 2d_1/c, \tau_2 = 2d_2/c$. The resultant amplitude and phase shift sensed by a ToF camera using modulation frequency f_0 are,

$$\begin{aligned} \tilde{a}(f_0) &= \sqrt{a_1^2+a_2^2+2\,a_1 a_2 \cos 2\pi f_0(\tau_1-\tau_2)} \\ \tilde{\tau}(f_0) &= \tan^{-1}\left(\frac{a_1 \sin 2\pi f_0\tau_1+a_2 \sin 2\pi f_0\tau_2}{a_1 \cos 2\pi f_0\tau_1+a_2 \cos 2\pi f_0\tau_2}\right) \end{aligned} \tag{11}$$

Assume without loss of generality (w.l.o.g), $\tau_1 < \tau_2$. Also physical laws dictate that $0 \leq a_1, a_2 \leq 1$. Under these conditions, it is easy to show that $\tau_1 \leq \tilde{\tau}(f_0) \leq \tau_2$. Sensor pixels corrupted with multipath, are often referred to as *flying* pixels (Figure 2). Other effects of multipath interference in ToF cameras include shape distortion at scene corners and flattening of curved objects.

The goal of MIC is to accurately detect the presence of multipath interference at a sensor pixel, and estimate the direct path distance, d_1, and amplitude, a_1, from samples $z_-[m;\tilde{\tau}]$. Clearly a single modulation frequency is not enough for detecting multipath and estimating the four multipath parameters. Multi-frequency based methods for MIC have been recently proposed [5] but these techniques are computationally complex since they involve solving a difficult, non-convex optimization problem. Other methods that use scene priors for multipath modeling and correction have also been recently proposed [13].

In the next section, we introduce SPUMIC, a low complexity method for joint PUW and MIC. Our technique is also based on multiple modulation frequencies for ToF acquisition.

4. SIMULTANEOUS PHASE UNWRAPPING AND MULTIPATH CANCELLATION

The key concept behind our method, SPUMIC, is formulation of PUW and MIC as line spectra estimation problems. To accomplish this, fix the modulation frequency, f, and use the two-path model defined in Equation 10 to compute sensor output described in Equation 5,

$$z_-(\phi, f) = a_1 \cos 2\pi f(\phi+\tau_1)+a_2 \cos 2\pi f(\phi+\tau_2) \tag{12}$$

Note the explicit dependence of sensor output on ϕ as well as the modulation frequency, f. SPUMIC is based on sampling the sensor output in both f and ϕ. First, fix $f = 1/T$ and sample $z_-(\phi, f)$ as before, i.e, at $\phi = mT/M; m = 0, \ldots, (M-1)$. Using the samples, $z_-[m, f)$, we define the complex phasor,

$$\mathrm{C}(f) = \frac{2}{M}\sum_{m=0}^{M-1} z_-[m, f) e^{j\frac{2\pi m}{M}} \tag{13}$$

Using simple algebraic manipulations, we show that the phasor $\mathrm{C}(f)$ is the sum of two complex exponentials, i.e.,

$$\mathrm{C}(f) = a_1\left(e^{j\,4\pi d_1/c}\right)^f + a_2\left(e^{j\,4\pi d_2/c}\right)^f \tag{14}$$

Equation 14 describes a line spectra model of order 2. This fact suggests sampling the phasor in four or more frequencies, f, and using spectral estimation techniques [14] to detect multipath interference and recover the multipath parameters, $\{a_1, a_2, d_1, d_2\}$. Note that no multipath $\iff a_2 = 0$.

Next, based on the above motivation we present our framework SPUMIC for joint PUW and MIC which uses spectral estimation and comprises the following steps:

4.1. Sampling and Data Acquisition

SPUMIC requires sampling the cross-correlation function (Equation 4) in both ϕ and f. For two-path MIC (Equation 10) we require that the number of frequency samples, $K \geq 4$ and since we are using sinusoidal modulation we require the number of phase samples, $M \geq 2$.

Our data acquisition is as follows: we pick a base modulation frequency, f_0, which governs the maximum aliased distance, $c/2f_0$, and a positive integer K_0 which governs the minimum modulation frequency, $K_0 f$. As mentioned before, higher modulation frequencies provide more accurate distance estimates but also leads to more phase wrapping. We modulate the ToF camera using K uniformly spaced modulation frequencies, $f = \{(K_0+k)f_0 : k = 1, \ldots, K\}$ and for value of f we acquire M samples of the cross-correlation function phase, ϕ. We collect a total of $K \times M$ samples denoted by $z_-[m, k]$. Next we discuss phase unwrapping and multipath detection and estimation using our data.

4.2. Parametric Spectral Estimation for PUW and MIC

We first discuss the noiseless recovery, described as follows:
Step 1. Compute phasors: Use samples, $z_-[m, k]$, to compute K complex phasors, one for each modulation frequency

$$\mathrm{C}[k] = \frac{2}{M}\sum_{m=0}^{M-1} z_-[m, k] e^{j\frac{2\pi m}{M}}, \quad k = 1, \ldots, K \tag{15}$$

Step 2. Detect multipath: For simplicity let $K = 2r+1$. Form a Hankel matrix of dimensions $r \times r$ using the K complex phasors, $\mathrm{C}[k]$. Compute the rank of this matrix, and if

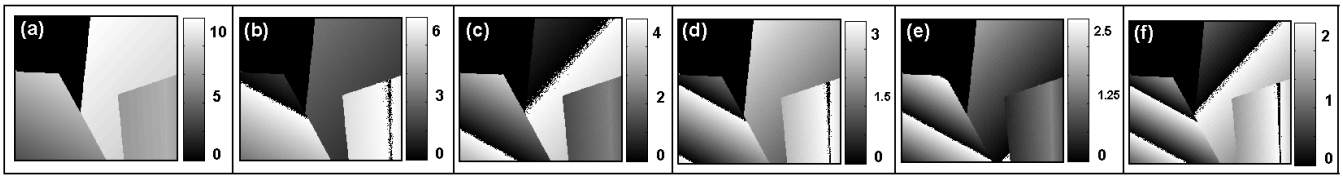

Fig. 3. Simulated data with SNR = 25 dB (a) Ground truth depth map. (b-f) Noisy, aliased depth map computed at modulation $f = 22, 33, 44, 55, 66$ MHz computed using the noisy samples. Note the values of maximum distances in each of the images (all values are in meters).

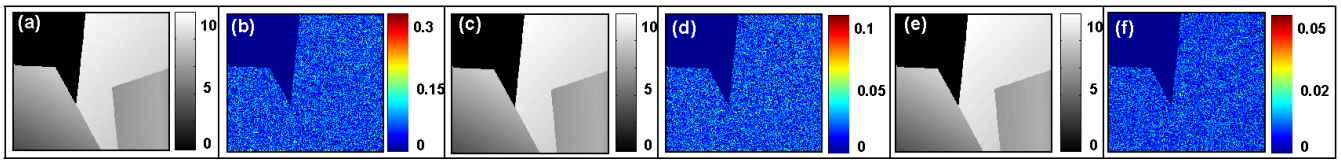

Fig. 4. (a) Noisy depth map acquired using a single, low modulation frequency, $f = 11$ MHz that does not have any aliasing. (b Error image for single frequency depth estimate with mean-square error (MSE) $= 29.9$ dB. (c, d) Depth map reconstruction using SPUMIC and the error image with an MSE $= 20.4$ dB. (e, f) Depth map reconstruction obtained using the maximum likelihood estimation described in Section 5 and the error image with an MSE $= 10.8$ dB.

rank ≥ 2, declare multipath else there is one direct path.

Step 3a. Parameter estimation with no multipath: As we will show shortly, in the absence of noise as well as multipath the amplitude estimate $\hat{a} = |\mathrm{C}[k]|$ and the unwrapped distance estimate is simply given by

$$\hat{d} = \frac{c}{4\pi f_0} \arg\left\{\frac{\mathrm{C}[k+1]}{\mathrm{C}[k]}\right\}, \text{ for any } k \geq 1 \qquad (16)$$

Step 3b. Multipath parameter estimation: If multipath is detected, then we employ the total least square (TLS) Prony's method [15, 14, 16, 17] to recover $\{d_1, d_2\}$. First we compute the nullspace eigenvector, $\mathbf{v}$ defined as the solution to the following Hankel system of equations,

$$\begin{bmatrix} \mathrm{C}[1] & \mathrm{C}[2] & \mathrm{C}[3] \\ \mathrm{C}[2] & \mathrm{C}[3] & \mathrm{C}[4] \\ \ddots & \ddots & \ddots \\ \mathrm{C}[K-2] & \mathrm{C}[K-1] & \mathrm{C}[K] \end{bmatrix} \begin{bmatrix} v_1 \\ v_2 \\ v_3 \end{bmatrix} = \mathbf{0} \qquad (17)$$

Then we compute the roots of the quadratic $v_1 + v_2\,\omega + v_3\,\omega^2$. It follows from spectral estimation theory [14] that $\omega_1 = e^{j\,4\pi f_0 d_1/c}$ and $\omega_2 = e^{j\,4\pi f_0 d_2/c}$ and hence we can easily recover estimates $\{\hat{d}_1, \hat{d}_2\}$. Finally the amplitude estimates are obtained by solving a Vandermonde least square system,

$$\begin{bmatrix} e^{j\,4\pi(K_0+1)f_0 d_1/c} & e^{j\,4\pi(K_0+1)f_0 d_2/c} \\ \vdots & \vdots \\ e^{j\,4\pi(K_0+1)f_0 d_1/c} & e^{j\,4\pi(K_0+K)f_0 d_2/c} \end{bmatrix} \begin{bmatrix} \hat{a}_1 \\ \hat{a}_2 \end{bmatrix} = \begin{bmatrix} \mathrm{C}[1] \\ \vdots \\ \mathrm{C}[K] \end{bmatrix} \qquad (18)$$

The algorithms described in Steps $1-3$ is precisely the Prony's method [15] for line spectra estimation applied to the problem of multipath parameters estimation, $\{a_1, a_2, d_1, d_2\}$. In the noiseless case, it is straight forward to show that using our proposed algorithm we perfectly recover amplitudes $\{a_1, a_2\}$ and distances $\{d_1, d_2\}$ within the maximum aliasing distance $c/2f_0$. In the noisy case we use robust versions of Steps $1-3$; for model order estimation and multipath detection we employ singular value based methods [14] and for multipath estimation, we use Cadzow's denoising procedure [16, 17] before computing estimates in Step 3. As shown in our next section, the robust version of SPUMIC achieves accurate phase unwrapping and multipath cancellation even in the presence of signal dependent noise.

5. SIMULATIONS AND RESULTS

The simulations are divided into two parts, one that evaluates the performance of SPUMIC for PUW and the other one that is an evaluation of SPUMIC for simultaneous PUW and MIC problems. All simulations were carried out at an SNR $= a/(a+b)$ of 25 dB with signal dependent additive Gaussian noise. All scene points were assumed to have a unit reflectance, i.e., $a = 1$ along with no radial-off attenuation. The five chosen frequencies were, $f = 22, 33, 44, 55, 66$ MHz. Using this choice of of modulation frequencies any method will be able to alias up to a distance of $c/(2\times 11MHz) \approx 13$ meters. At each frequency, the cross-correlation function was sampled at four values of $\phi = 0,\ \pi/4,\ \pi/2,\ 3\pi/4$.

5.1. Phase Unwrapping results:

Figures 3 and 4 show simulations results comparing the performance of SPUMIC with two other methods:
1. Depth acquisition using a single, low modulation frequency that does not cause any aliasing. In our case, this frequency was chosen to be $f = f_0 = 11$ MHz, and,
2. The nonconvex maximum likelihood depth estimate at each pixel which is defined as the value the minimizes the least square error between the model and data,

$$\hat{d}_{ML} = \arg\min_{d} \sum_{\phi} \sum_{f} \left[z_{-}(\phi, f) - \cos 2\pi f(\phi + 2d/c)\right]^2 \qquad (19)$$

As shown in Figure 4, the performance of SPUMIC is better than using a single modulation frequency to estimate depth. This gain explained by the fact that more samples at other

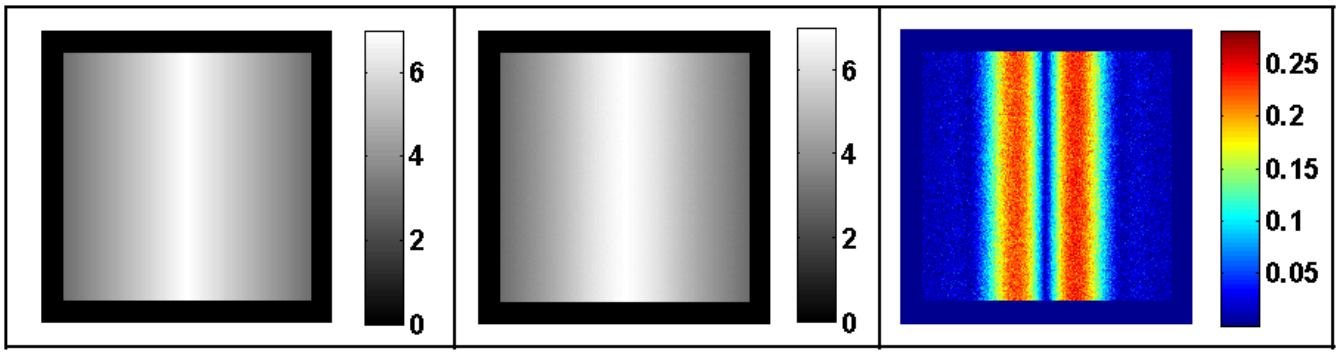

Fig. 5. (Left) Ground truth depth map of scene shown in Figure 6. (Center) Depth map computed using single, low modulation frequency of $f = 11$ MHz. (Right) The absolute error image shows the multipath error pattern. Multipath error due to diffuse inter-reflection increases at first, but again decreases because the direct and second path lengths become close near the wedge center. MSE = 28.5107 dB at an SNR = 25 dB. All units are in meters.

frequencies allow for a robust estimation of depth. The performance of SPUMIC is not as good as the maximum likelihood (ML) estimate. The use of high resolution frequency estimation methods like matrix pencil and ESPRIT could allow SPUMIC to achieve performance comparable to the ML estimate. Also note that the ML problem is non-convex and in general it is difficult to guarantee global minimum solutions unless we use methods with higher computational complexity such as grid search followed by Newton descent. Compared to the high computational complexity of ML, and the poor performance of single frequency methods, SPUMIC offers a intermediate solution which has both good performance as well as low computational complexity.

5.2. Joint Multipath Interference Cancellation and Phase Unwrapping:

Figures 6 shows the scene setup for the multipath interference simulations. The scene is a wedge shaped object and suffers for multipath interference due to inter-reflections of light. A sensor pixel receives two contributions, a direct path (shown in solid arrow) and a delayed and attenuated second path (dotted arrow). Thus the estimated single path depth is an erroneous estimate of the true, direct depth value. Our goal is to recover the estimate of the direct and shorter first path.

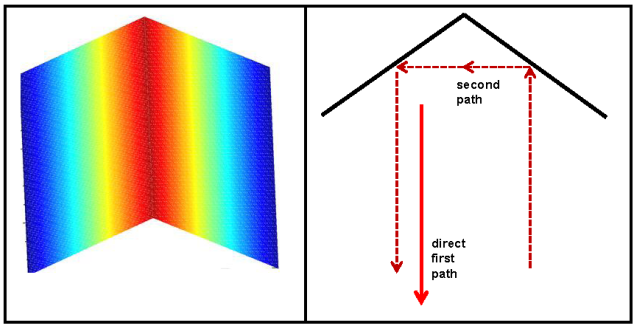

Fig. 6. Scene setup for multipath simulations. The closest depth in deep blue is 3 meters and the farthest depth in red is 6 meters. The vertical and horizontal dimensions are chosen to be 8 meters.

As shown in Figure 5, the multipath error is high near the intersection of the two surfaces. The multipath error is computed as a difference of the ground truth image and the single path estimated obtained using a single, low modulation frequency, $f = f_0 = 11$ MHz. The edges of the wedge suffer from very little multipath interference due to decaying strength of the diffuse inter-reflections.

Figure 7 shows the performance of SPUMIC for simultaneous phase unwrapping and multipath interference cancellation. The goal of SPUMIC is two-fold:
1. Detect the presence of multipath. This is done by computing the singular values of the Hankel matrix as described in Section 4.2. We found that the ratio of the second singular value to the first one is a good indicator of the presence of multipath as well as the amount of multipath. As shown in Figure 7(left) the ratio of singular values is very well correlated with the amount of multipath error, even in the presence of noise (SNR = 25 dB).
2. Multipath parameter estimation. Using a simple thresholding scheme on the ratio of singular values, we first detect multipath and then use Cadzow's method to denoise the data before estimating the direct and second path distances and amplitudes. The corrected distance values as well as the error image indicate a significant reduction in the multipath error. The center of the wedge remains a tough area to correct for multipath interference.

6. DISCUSSION AND CONCLUSION

We presented a new framework for simultaneous phase unwrapping and multipath interference cancellation in homodyne TOF cameras. These two problems are two of the main challenges in improving the imaging quality of TOF cameras. Several methods have been proposed for individually solving each of the two problems but no joint framework exists as per as our knowledge. Moreover, all of the proposed methods typically either use image or scene priors and are computationally intensive. Our method, SPUMIC, is a pointwise estimator

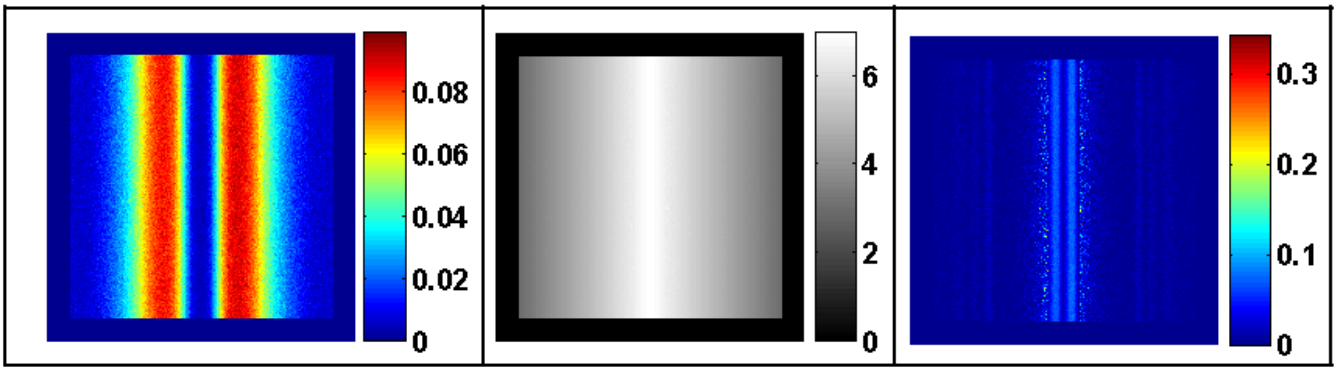

Fig. 7. (Left) Ratio of the first and second singular value of the Hankel matrix constructed using the correlation samples. Note the high correlation between this figure and Figure 5 (right). (Center) Unwrapped, direct path depth map computed using SPUMIC. (Right) The absolute error image shows significant reduction in the multipath error in the reconstructed depth map that contains only the first, shortest path depth values. MSE = 14 dB at an SNR = 25 dB.

that allows both multipath interference as well as phase unwrapping at very low computational complexity. However, it requires more number of captures or samples to be collected. An increasing number of TOF cameras are supporting multiple modulation frequencies. On such cameras, our technique will be immediately applicable without requiring any hardware modifications.

Our future work involves more extensive simulations to validate estimator performance on a variety of scenes. We will also carry out experiments with data acquired from commercial TOF imagers. On the theoretical side, it is important to develop robust versions of SPUMIC that may use high resolution spectral estimation techniques like matrix pencil, MUSIC and ESPRIT. We will also derive Cramér-Rao bounds for both multipath detection based on our method of using singular value ratios, and for the estimation problem of computing multipath parameter values.

7. REFERENCES

[1] A. Kolb, E. Barth, R. Koch, and R. Larsen, "Time-of-flight sensors in computer graphics," in *Proc. Eurographics (State-of-the-Art Report)*, 2009.

[2] S.B. Gokturk, H. Yalcin, and C. Bamji, "A time-of-flight depth sensor-system description, issues and solutions," in *Computer Vision and Pattern Recognition Workshop, 2004. CVPRW'04. Conference on*. IEEE, 2004, pp. 35–35.

[3] J.P. Godbaz, M.J. Cree, and A.A. Dorrington, "Closed-form inverses for the mixed pixel/multipath interference problem in amcw lidar," in *IS&T/SPIE Electronic Imaging*. International Society for Optics and Photonics, 2012, pp. 829618–829618.

[4] M. Frank, M. Plaue, H. Rapp, U. Köthe, B. Jähne, and F.A. Hamprecht, "Theoretical and experimental error analysis of continuous-wave time-of-flight range cameras," *Optical Engineering*, vol. 48, no. 1, pp. 013602–013602, 2009.

[5] D. Droeschel, D. Holz, and S. Behnke, "Multi-frequency phase unwrapping for time-of-flight cameras," in *IEEE/RSJ*, 2010, pp. 1463–1469.

[6] C. Ye, "Mixed pixels removal of a laser rangefinder for mobile robot 3-d terrain mapping," in *Information and Automation, 2008. ICIA 2008. International Conference on*. IEEE, 2008, pp. 1153–1158.

[7] A.A. Dorrington, J.P. Godbaz, M.J. Cree, A.D. Payne, and L.V. Streeter, "Separating true range measurements from multi-path and scattering interference in commercial range cameras," in *IS&T/SPIE Electronic Imaging*, 2011, pp. 786404–786404.

[8] S. Fuchs, "Multipath interference compensation in time-of-flight camera images," in *Pattern Recognition (ICPR), 20th International Conference on*. IEEE, 2010.

[9] D. Jiménez, D. Pizarro, M. Mazo, and S. Palazuelos, "Modelling and correction of multipath interference in time of flight cameras," in *Computer Vision and Pattern Recognition (CVPR)*, 2012, pp. 893–900.

[10] T. Edeler, K. Ohliger, S. Hussmann, and A. Mertins, "Time-of-flight depth image denoising using prior noise information," in *proceedings ICSP*, 2010, pp. 119–122.

[11] F. Mufti and R. Mahony, "Statistical analysis of measurement processes for time-of-flight cameras," in *Proceedings of SPIE*, 2009, vol. 7447, p. 74470I.

[12] D.L. Snyder, "Random point processes," 1975.

[13] M. Reynolds, J. Dobos, L. Peel, T. Weyrich, and G.J. Brostow, "Capturing time-of-flight data with confidence," in *Computer Vision and Pattern Recognition (CVPR), 2011 IEEE Conference on*. IEEE, 2011, pp. 945–952.

[14] P. Stoica and R.L. Moses, *Introduction to spectral analysis*, vol. 89, Prentice Hall Upper Saddle River, NJ, 1997.

[15] R. Prony, "Essai experimental–,-," *J. de l'Ecole Polytechnique (Paris)*, vol. 1, no. 2, pp. 24–76, 1795.

[16] T. Blu, P.L. Dragotti, M. Vetterli, P. Marziliano, and L. Coulot, "Sparse sampling of signal innovations," *Signal Processing Magazine, IEEE*, vol. 25, no. 2, pp. 31–40, 2008.

[17] P.L. Dragotti, M. Vetterli, and T. Blu, "Sampling moments and reconstructing signals of finite rate of innovation: Shannon meets strang–fix," *Signal Processing, IEEE Transactions on*, vol. 55, no. 5, pp. 1741–1757, 2007.